Sensors and Actuators B 238 (2017) 473–481

Contents lists available at ScienceDirect

Sensors and Actuators B: Chemical

journal homepage: www.elsevier.com/locate/snb

NH_3 gas sensing performance enhanced by Pt-loaded on mesoporous WO_3

Yinglin Wang[a,b], Jie Liu[b], Xiaobiao Cui[b], Yuan Gao[b,*], Jian Ma[b], Yanfeng Sun[b], Peng Sun[b], Fengmin Liu[b], Xishuang Liang[b], Tong Zhang[b], Geyu Lu[a,b,*]

[a] State Key Laboratory of Automotive Simulation and Control, Jilin University, 2699 Qianjin Street, Changchun 130012, China
[b] State Key Laboratory on Integrated Optoelectronics, College of Electronic Science and Engineering, Jilin University, 2699 Qianjin Street, Changchun 130012, China

ARTICLE INFO

Article history:
Received 12 May 2016
Received in revised form 8 July 2016
Accepted 17 July 2016
Available online 19 July 2016

Keywords:
Pt
WO_3
Hard template
Mesoporous
Ammonia

ABSTRACT

Pt-loaded mesoporous WO_3 was fabricated by nanocasting method. Mesoporous structure provided ordered tunnel which was convenient for gas diffusion and the large specific surface area which could offer more active sites. The noble metal (Pt) improved the catalytic efficiency which played crucial role in enhancing the performance of the gas sensor. The obtained materials were characterized by X-ray diffraction (XRD), Brunauer-Emmet-Teller (BET), Transmission electron microscopy (TEM) and X-ray photoelectron spectroscopy (XPS). Characterization indicated that the synthesized materials had ordered mesoporous structure with excellent crystallinity and the pore size was about 10.6 nm. Static test system was employed to measure ammonia sensing properties for the as-prepared samples. The sensor based on Pt-loaded WO_3 presented higher sensitivity, quicker response-recovery rates, excellent repeatability and selectivity. It indicated that the Pt-loaded mesoporous WO_3 was a potential ammonia gas sensor material.

1. Introduction

Global environmental issues caused by kinds of released chemical pollutants have attracted widespread attention. Ammonia (NH_3) as a kind of reducing and colorless gas with special odor is a major air contamination produced from agricultural practices, industrial emissions and refrigerators [1]. Its long-term exposure and inhalation to higher concentrations >5000 ppm can cause serious health problems and even lead to death [2]. The American National Institute for Occupational safety and Health has set up the safety standard towards NH_3 and the limitation of immediately dangerous to life or health concentration (IDLH) is stipulated to be 300 ppm. Owing to the low density and volatile nature of ammonia, the affected area is quite large once a leakage of ammonia has happened [3]. Therefore, the increasing demand of detecting low ammonia concentration under low temperature is urgency in many areas, such as food technology, chemical engineering, medical diagnosis and industrial process.

Extensive efforts on research of new sensors have been carried out to detect and forewarning NH_3 gas such as electrochemical sensors [4], optical sensors [5,6] and SAW (surface acoustic wave) sensors [7,8]. In the sensors above, sensing materials play vital roles in sensing performance. Some promising sensing materials, such as SnO_2, ZnO, WO_3 and CuBr [9,10], have been reported applied in NH_3 gas sensors. However, among the numerous materials, metal oxide semiconductor (MOS) materials have gained great focus on a global scale for the simple design structure and low cost. The abundant microstructural defects exist in MOS are beneficial for the formation of absorbed oxygen ions [11,12]. WO_3 as an n-type MOS is promising and frequently used as sensing material, because it shows unique sensing properties to NO_2 and reducing gases. Furthermore, WO_3 can also detect NH_3 even in the presence of other gases such as H_2, CO and CH_4 [13]. Some of attempts have been devoted to fabricated WO_3 gas sensor with optimizing sensitivity, selectivity, response rate and long-term stability. And some of efforts have been exert on obtaining pure or transition metal doped nanostructured [14], mesoporous [15] and macroporous [16] WO_3 based materials.

Mesoporous materials based on metal oxides have become strategic for sensor devices due to the lightweight, high surface area and the well-defined porous architecture. High surface area favors the gas-oxide interaction [17,18], moreover, the mesoporous struc-

* Corresponding authors at: State Key Laboratory on Integrated Optoelectronics, College of Electronic Science and Engineering, Jilin University, 2699 Qianjin Street, Changchun 130012, China
E-mail addresses: gaoyuan@jlu.edu.cn (Y. Gao), lugy@jlu.edu.cn (G. Lu).

http://dx.doi.org/10.1016/j.snb.2016.07.085
0925-4005/

ture significantly improve gas diffusion throughout the porous and consequently the sensing performance [18]. To further improve the gas response, noble metals (such as Pd, Pt and Ag) have been applied to modify the sensing material to enhance the catalytic reaction with the target gas [19,20]. High response and selectivity of WO_3 doped with Pd to H_2 gas was reported at a working temperature of 200 °C [21]. Morazzoni and co-workers reported that Pt homogeneously dispersed into the oxide matrix, which could catalyze the electron transfer between gas molecules and the semiconductor [22]. These indicated that the noble metals in such materials act as catalysts of the chemical interaction between gas molecule and the semiconductor [23].

In our present work, we described a simple impregnation route to load different weight percent of Pt (0.2%, 0.5% and 1.0%) into mesoporous WO_3 samples for NH_3 sensing purpose. Nanocasting was adopted to prepare mesoporous WO_3 by replicating the structure of hard template. The highly ordered mesoporous structure was observed with average pore diameter about 10 nm, and a high specific surface area (85.8 $m^2\ g^{-1}$) was obtained. The gas sensors fabricated with the obtained materials presented good sensing performance toward NH_3. Working at a temperature as low as 125 °C, the gas response of 1.0% Pt-loaded mesoporous WO_3 to 200 ppm of NH_3 reached as high as 13.6. The structure, morphology and chemical state were also investigated to give a further understanding. Moreover, the related mechanism of gas sensing would be illustrated in this paper.

2. Experimental details

All the chemical reagents used in the experiments were obtained from commercial sources as guaranteed-grade reagents and were without further purification.

2.1. Preparation

The three-dimension ordered mesoporous silica KIT-6 was prepared in acidic condition using a mixture of Pluronic P123 as structure directing agent and butanol. 6 g of P123, an amphiphilic triblock copolymer of $EO_{20}PO_{70}EO_{20}$, was firstly dissolved in 217 g deionized water, and then diluted 37 wt% aqueous HCl solution was mixed with 6 g of *n*-butanol at 35 °C by stirring 1 h. 12.9 g of tetraethylorthosilicate (TEOS) was subsequently added into the system and vigorous stirring for 24 h. The obtained mixture were placed in an autoclave and heated for 24 h at 100 °C under static conditions. The prepared white precipitant powder was further dried at 100 °C after filtering and washing using deionized water, and subsequently calcined at 550 °C for 6 h.

The mesoporous WO_3 was prepared by nanocasting method using the above mesoporous KIT-6 as the template and phosphotungstic acid as the tungsten precursor. 0.5 g of KIT-6 and 0.7 g of phosphotungstic acid were mixed in 25 mL of ethanol, the obtained slurry was stirred at 40 °C till all the solvent was evaporated further followed by calcination at 300 °C for 2 h. The mixture of silica and oxide was dissolved again in ethanol with 0.35 g of W precursor for second impregnation and calcined for another 2 h at 300 °C. Sequentially, the resultant mixture was solved again in ethanol with 0.15 g of phosphotungstic acid, dried at 40 °C and calcined at 500 °C for 2 h. Finally the KIT-6 was removed with HF (2 mol/L) for the WO_3 materials. The as-prepared slurry was centrifuged, washed at room temperature and dried at 80 °C.

Different weight percent of Pt (0.2%, 0.5% and 1.0%) was loaded in nanocasted WO_3 by wet impregnation method. Chloroplatinic acid as Pt precursor was dissolved in the mixture of mesoporous 0.3 g of WO_3 and 20 mL ethanol. The slurry was dried at 40 °C and followed by calcination at 300 °C for 2 h, and the mesoporous Pt-loaded WO_3 was obtained.

2.2. Characterization

The crystallinity and phase of the sensor materials were characterized by X-ray diffraction (XRD, Rigaku D/MAX-2550), where Cu-Kα radiation ($\lambda = 0.15418$) was used for the X-ray source and the diffracted X-ray intensities were recorded as a function of 2θ. N_2 adsorption-desorption isotherms were measured with a Micrometrics Gemini VII surface area and porosity system by high purity nitrogen as adsorbate at 77 K. The specific surface area was estimated by the five points Brunauer-Emmet-Teller (BET) method, and the pore size distribution was obtained by using the Barrett-Joyner-Halenda (BJH) analysis. The samples were degassed under vacuum at 200 °C for several hours prior to the measurement. Transmission electron microscopy (TEM) and high resolution transmission electron microscopy (HRTEM) characterization were performed with a JEOL TEM-2100 instrument at an acceleration voltage of 200 kV. The samples for TEM were prepared by dispersing the final dry powders in ethanol; these dispersions were then dropped on carbon-copper grids. X-ray photoelectron spectroscopy (XPS) was carried out at room temperature on Thermo ESCALAB 250 spectrometer. During the XPS analysis, an Al Kα X-ray beam was adopted as the excitation source. The measurement spectra were decomposed into Gaussian components by a least-square fitting method. The binding energies ($\pm$0.2 eV) were calibrated with reference to the C 1s peak (284.8 eV).

2.3. Fabrication and measurement of the gas sensor

The sensor was fabricated in accordance with the literature [24]. The obtained samples were mixed with an appropriate amount of deionized water to form a paste. Later on, the paste was coated onto the outside surface of an alumina ceramic tube (4 mm in length, 0.8 mm in inner diameter and 1.2 mm in outer diameter, attached with Pt wires on a pair of Au electrodes). The gas sensing material was covered on the whole surface of the Au electrodes to guarantee good contact. The products were sintered at 300 °C after dried under IR radiation. Ni-Cr alloy coil was subsequently inserted into the alumina tube as a heater to control the operating temperature. In order to improve the stability and repeatability, the fabricated sensor was aged at 200 °C for 72 h in air. The gas sensing properties were measured with a RQ-2 characterization system under laboratory conditions (50 ± 2% RH, 25 ± 1 °C). The measurement was processed by a static process: the desired amount of target gas was injected into the test gas chamber for the measurement of sensing performance, afterwards atmosphere air was drew into the test gas chamber as background gas, and the sensor was put into the test chamber for the measurement of the sensitive performance. The gas response was defined as $S = R_a/R_g$ (reducing gas) and $S = R_g/R_a$ (oxidizing gas), where R_a and R_g were the resistance in air and the target gas, respectively. In addition, the response time was defined as the time required for the gas response to reach 90% of the final equilibrium value after test gas was injected, and the recovery time was the time needed for the gas response to decrease to 90%, from the final equilibrium value, after the gas sensor was exposed to air again.

3. Results and discussion

3.1. Structure and morphology characterizations of obtained materials

X-ray diffraction analysis of the obtained materials is carried out for phase identification, and the results are shown in Fig. 1. As

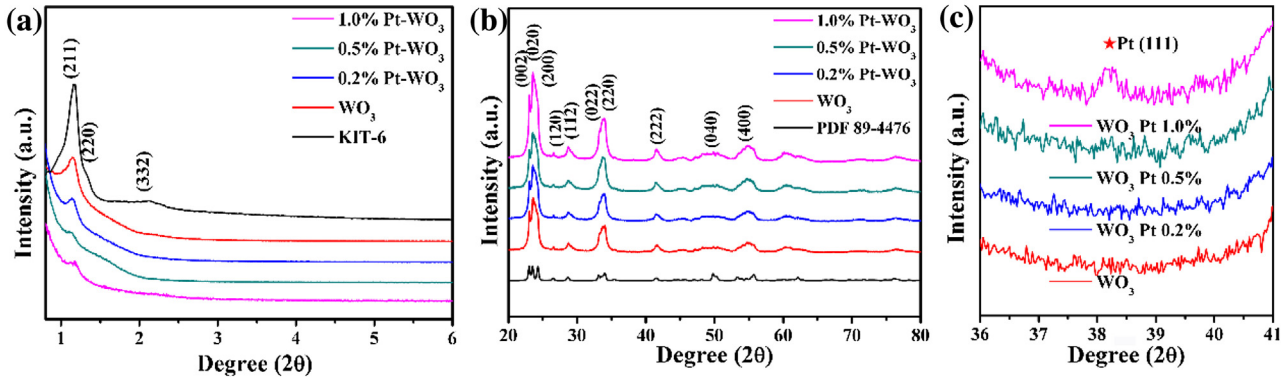

Fig. 1. XRD curves of obtained materials (WO_3, 0.2% Pt-WO_3, 0.5% Pt-WO_3, 1.0% Pt-WO_3): (a) low-angle patterns of materials (KIT-6 as reference pattern); (b) wide-angle patterns of materials (WO_3 PDF 89-4476 as reference pattern); (c) partial enlarged details of Fig. 1(b). (For interpretation of the references to colour in the text, the reader is referred to the web version of this article.)

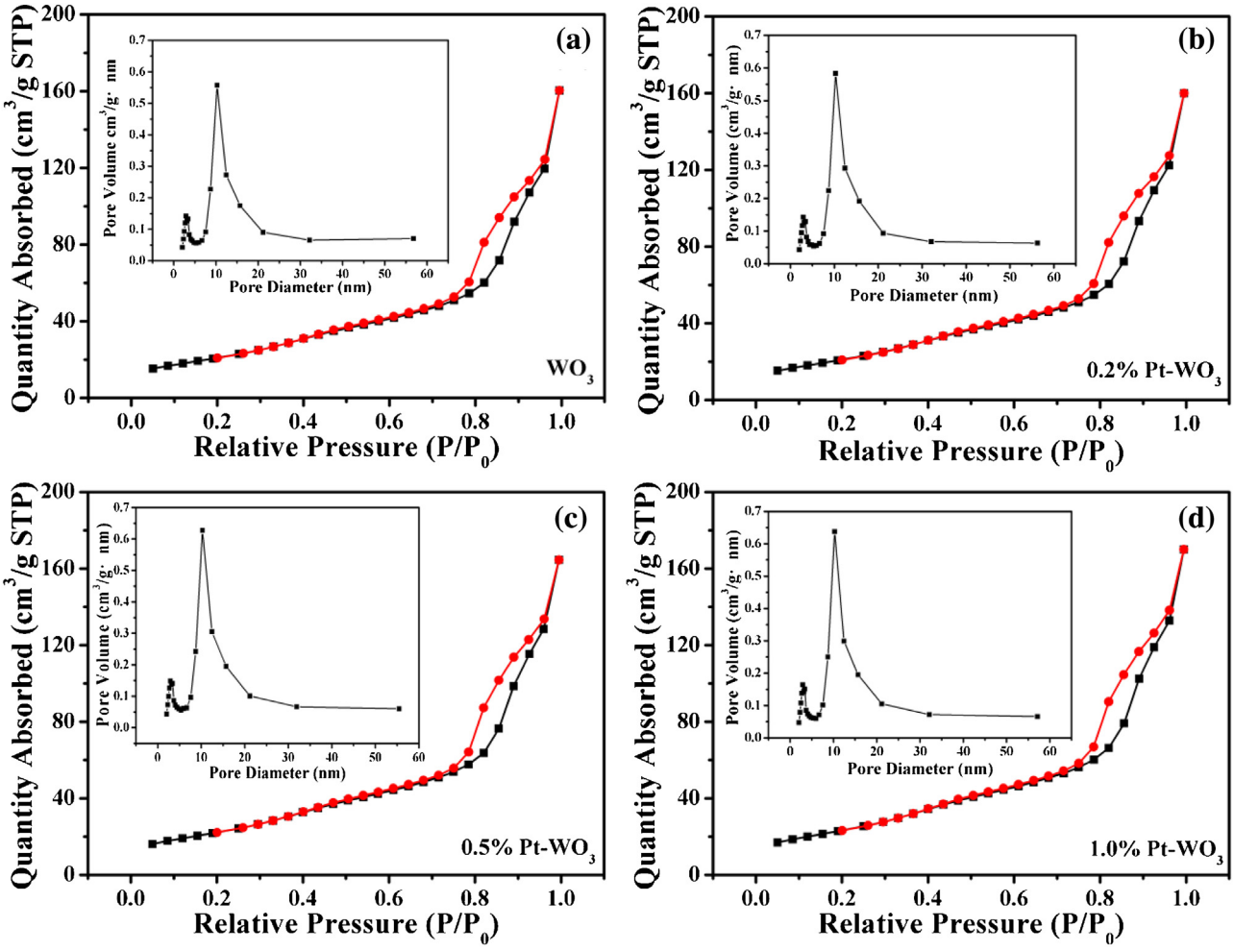

Fig. 2. Nitrogen adsorption-desorption isotherms of obtained mesoporous materials and the corresponding pore size distribution (—■— adsorption, ——●—— desorption). (a) WO_3, (b) 0.2% Pt loaded WO_3, (c) 0.5% Pt loaded WO_3 and 1.0% Pt loaded WO_3. (For interpretation of the references to colour in this figure legend, the reader is referred to the web version of this article.)

displayed in Fig. 1(a), each low-angle XRD pattern of the obtained material presents a sharp diffraction peak and two barely visible peaks accordance with silica template KIT-6. The peaks of (211), (220) and (332) reflect the ordered three-dimensional cubic mesostructure of obtained materials. The peaks of each materials occur at almost the same degree indicates the successful replication from the silica template. With the increasing of Pt content loaded in mesoporous WO_3, the peaks of obtained materials slightly move towards the higher degree. This phenomenon is on account of Pt loading in mesoporous framework which is obviously reflected from a decreased pore diameter. However, with the comparison of silica template KIT-6, the corresponding replica present somewhat lower intensity diffraction peaks, which means a slightly lower overall nanostructural order as frequently found for repli-

Table 1
The textural properties of mesostructured samples.

Sample	Surface area (m^2/g)	Average pore size (nm)	Pore volume (cm^3/g)
WO_3	77.45	10.09	0.2493
0.2% Pt-WO_3	77.89	9.98	0.2485
0.5% Pt-WO_3	82.05	9.75	0.2557
1.0% Pt-WO_3	85.82	9.65	0.2663

cated materials [25]. Fig. 1(b) presents the wide-angle XRD patterns of mesoprorous materials, obviously all the peaks of the patterns can be identified as the reflections of monoclinic tungsten oxide (JCPDS Card No. 89-4476) [26] with lattice parameters a = 7.327 Å, b = 7.564 Å and c = 7.727 Å. The XRD patterns of obtained samples reveal the characteristic peaks at 2θ value of 23.12°, 23.59° and 24.38° which are indexed to the diffractions of the (002), (020) and (200) planes of monoclinic WO_3, respectively. Fig. 1(c) reveals the partial enlarge details of wide-angle patterns of obtained materials, from which a low intensity peak (marked with red asterisk) occurs at 2θ value of 38.75° of 1.0% Pt-loaded WO_3 sample correspond to the (111) planes of the cubic Pt phase (JCPDS Card No. 01-1174, lattice parameter a = 4.028). However, no reflection peak indexed Pt can be found from the pattern of other sample loaded with Pt, which may be caused by the low amount of Pt loaded in the mesoporous WO_3 or a homogenous distribution of Pt particles [24].

Nitrogen physisorption experiments are performed on all the prepared mesoporous materials. The adsorption-desorption isotherm and corresponding pore-size distribution of obtained materials are shown in Fig. 2. The mesoporous sample shows a type IV Brunauer isotherm with a capillary condensation occurring in the relative pressure (P/P_0) of 0.7–1.0 in the high pressure region. The isotherms obtained for the prepared samples show H1 hysteresis loops which are typical characteristics of materials with mesoporous structure. The curves of insets in Fig. 2 reveal the distribution of pore size conditions with two peaks occur at about 3 nm and 12 nm, respectively. The one peak occurs at 3 nm is tensile strength effect (TSE) peak, the other peak occurs at 12 nm is a most probable distribution peak. The average BET specific surface area, BJH pore size distribution and pore volume of samples are reported in Table 1. The obtained BET surface areas provided by samples are in the range of 77–85 m^2/g, which confirms the mesoporous materials with large surface area have been fabricated successfully. In details, the surface area increases with the increasing of Pt concentration, which may be caused by the incorporation of Pt attached on the WO_3 framework affects the integrity and mesostructure [24]. The increasing crystallinity of Pt loaded in mesoporous framework may also contribute to the increasing surface area. The pore size

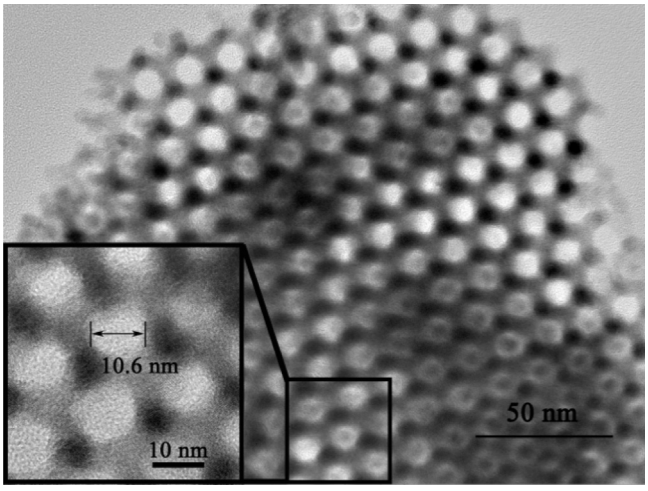

Fig. 3. TEM image of mesoporous WO_3 material prepared by nanocasting.

of materials mentioned in Table 1 is all around 10 nm, which is the average pore size distinguished from the most probable statistic method in Fig. 2. Comparatively, the broad pore size appeared among the materials may due to the slightly soluble of WO_3 in HF in the process of removal silica template. With the increasing content of Pt, the average pore size become small may be caused by the impregnation of Pt precursor. Although there are subtle distinctions, the fabricated samples possess the similar surface area, pore size and pore volume, which indicate the fabricate process has barely influence on the mesostructured of materials.

Detailed mesostructure features of prepared materials are further investigated by transmission electron microscopy (TEM). Fig. 3 shows the distinguishable periodic ordered mesoporous structure matched well with the mesoporous replication silica template KIT-6. This feature suggests that WO_3 particles assemble together inside the pore of the hard template. The TEM image of the edge part marked by the black line is magnified as the inset image in Fig. 3. It reveals that the mesoporous WO_3 possesses mesopores with average pore size about 10.6 nm which is corresponded with BET result. The TEM and high resolution TEM (HRTEM) images of the 1.0% Pt loaded on the mesoprous WO_3 are shown in Fig. 4(a). It can be observed that the ordered mesoporous structure still exists after the impregnation of Pt, which indicates that the Pt loading does not disturb the WO_3 assemble. The inset of HRTEM image presents the clear well-developed lattice fringe of material. The crystallographic planes (111) of platinum (JCPDS Card No. 87-644) and (020) of monoclinic WO_3 (JCPDS Card No. 89-4476) are observed with the corresponding lattice distance of 0.232 nm and 0.378 nm,

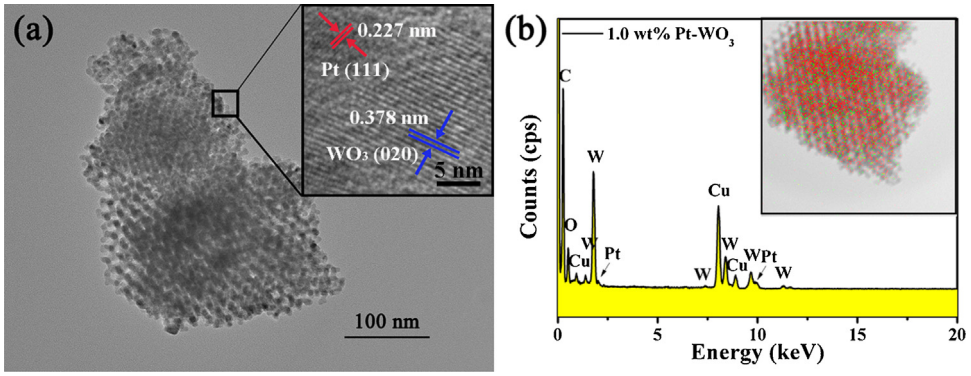

Fig. 4. (a) TEM and HRTEM images of 1.0% Pt loaded mesoporous WO_3, (b) energy dispersive analysis of 1.0% Pt loaded mesoporous WO_3 (W element represented in red color and Pt in green). (For interpretation of the references to colour in this figure legend, the reader is referred to the web version of this article.)

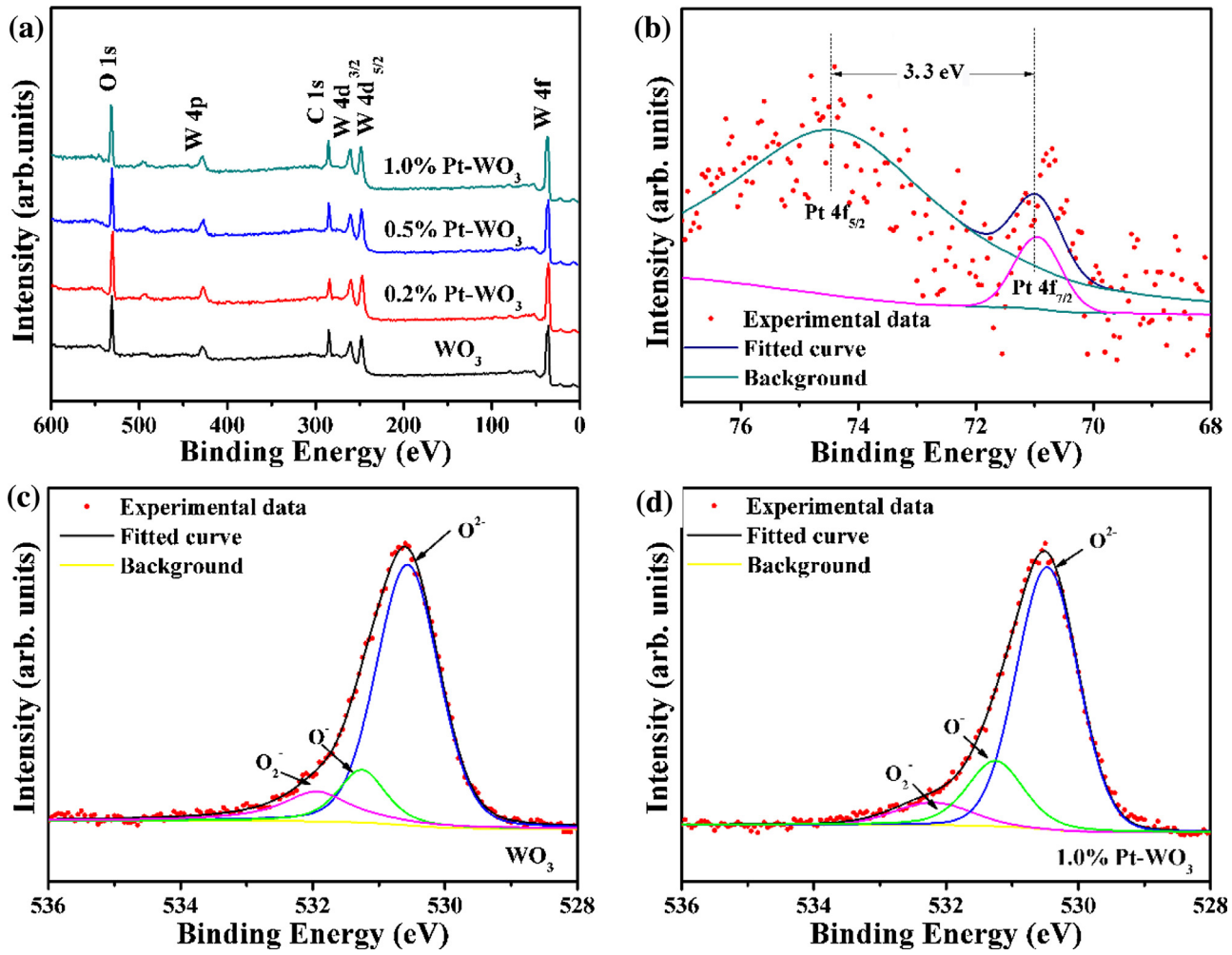

Fig. 5. XPS spectra of the obtained mesoporous materials: (a) survey scans of all the samples, (b) Pt spectrum of mesoporous WO_3 loaded with 1.0% Pt, (c) O 1s spectrum of pure mesoporous WO_3, (d) O 1s spectrum of mesoporous WO_3 loaded with 1.0% Pt.

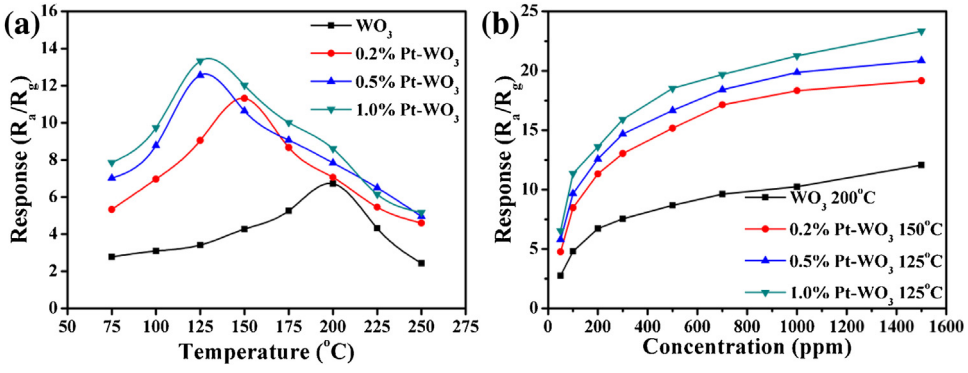

Fig. 6. (a) The sensor sensitivity of obtained materials towards 200 ppm of NH_3 as a function of the operating temperature; (b) the dot-line gas response patterns of the obtained samples to NH_3 with different concentration under each optimum operating temperature.

respectively. The energy spectrum and the distribution of Pt and W elements are exhibited in Fig. 4(b). W element as the "mother phase" presents high intensity peak, and concentration of Pt is low which presents weak intensity peak in the EDX spectrum. In addition, Cu and C signals are associated with the carbon-coated Cu grid that supports the prepared materials [27]. Pt element (marked with green color) is dispersed uniformly observed in inset of Fig. 4(b), and there is no indication of aggregation phenomenon, which confirms Pt is successfully loaded on the mesoporous WO_3 (marked with red color).

The composition and the chemical state of the elements existed in the surface of obtained materials are performed by XPS as shown in Fig. 5. The main structures in the spectra are analyzed and reproduced at the background of Shirley. The surface of prepared mesoporous materials are obviously composed of tungsten and oxygen elements in Fig. 5(a). As shown in Fig. 5(b), the high resolution spectrum of 1.0% Pt-loaded WO_3 demonstrates peaks occur

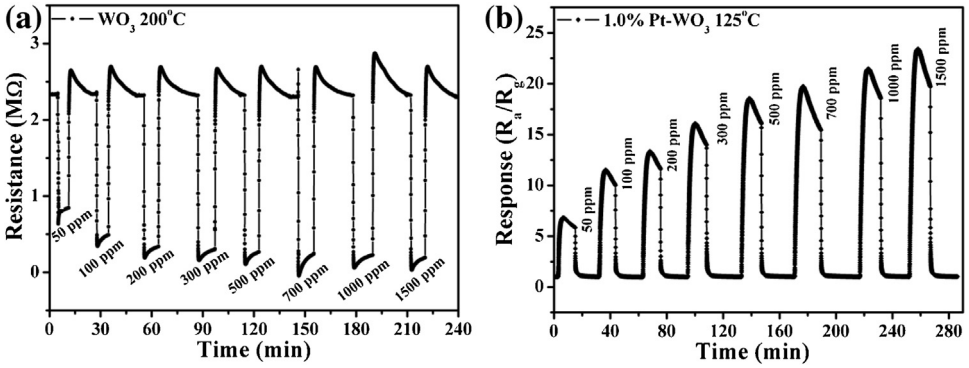

Fig. 7. Dynamic response-recovery characteristic curve of obtained mesoporous materials towards different ammonia concentration from 50 to 1500 ppm: (a) resistance curve of pure WO_3, (b) response curve of 1.0% Pt-loaded WO_3.

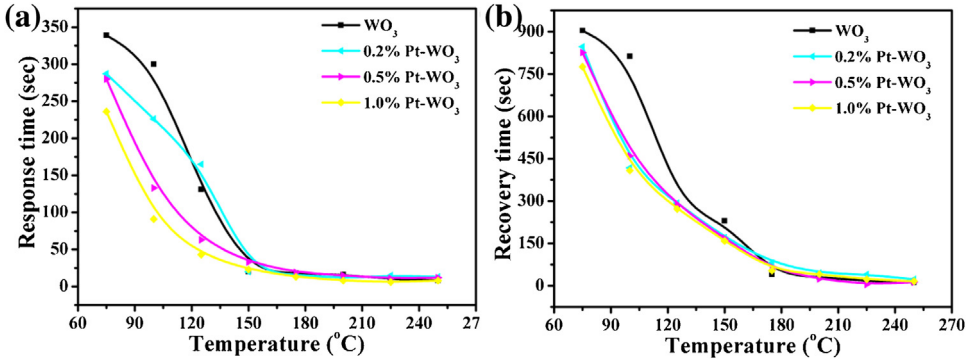

Fig. 8. Variation in (a) response time and (b) recovery time for the prepared mesoporous materials as a function of temperature towards 200 ppm ammonia.

at 74.42 eV and 71.10 eV (gap = 3.3 eV) which are assigned to Pt $4f_{5/2}$ and Pt $4f_{7/2}$, respectively. These values are in good agreement with the platinum metal [28]. Pt 4f band shape and peak position indicated that platinum is dispersed as the form of Pt (0) centers only [29]. However, from Fig. 5(a), the peak presents Pt element can barely be visible in the whole spectrum which may due to the high intensity of other element peaks submerge the Pt peak. The high resolution XPS spectrum of O 1 s in Fig. 5(c) and (d) could be resolved to three Gaussian function peaks with the energy of ~530.5 eV, ~531.2 eV and ~531.9 eV, which are attributed to three kinds of oxygen species on the surface of the mesoporous material. The first was lattice (surface) oxygen O^{2-}, the second was a dissociative type O^-, and the third was a molecular-type adsorbate O_2^-. O^- adsorbate, occupies more percentage in the case of 1.0% Pt-loaded WO_3, is more important than others [30]. O^{2-} is attributed to the oxygen ions in the crystal lattice which is thought to be pretty stable and have no contribution to the gas response. However, O_x^- is attributed to the adsorbed oxygen ions in the oxygen deficient regions [31], which have a significant role in the gas sensing property. Compared Fig. 5(c) with Fig. 5(d), the O_x^- in 1.0% Pt-loaded WO_3 is more than pure mesoporous WO_3, which may due to an interaction of ion-adsorbed oxygen with Pt (0). The existence of Pt (0) can be confirmed by the results of XRD patterns, TEM images and XPS spectra.

3.2. Gas sensing performances

To evaluate the potential applicability in gas sensors for ammonia, some fundamental gas sensing properties of the obtained materials are investigated. As is well known, the operating temperature has a great influence on the sensitivity of semiconductor based gas sensor, as it governs the mobility of electron and the electrical conductivity of the metal oxide material [32]. There usually exists a temperature region in which the sensor shows the highest response. Fig. 6(a) depicts the variation sensor sensitivity of the samples to 200 ppm of ammonia with the increasing operation temperature. It is obvious that all the response curves of the samples present bell-shape in the range of 75 °C–250 °C, besides the Pt-loaded materials present much higher responses. The gas response to 200 ppm of ammonia is enhanced from 6.72 for pure mesoporous WO_3 to 13.61 for 1.0% Pt-loaded WO_3 through the activation of Pt. In addition, the optimum operating temperature is shift from 200 °C to 125 °C. The decreased operation temperature may be caused by the catalyst of Pt. When the concentration of Pt is small, Pt dispersed on the part of inner surface of materials, the catalyst cannot catalyze all the target gas (NH_3). Some thermal energy still needed to active the interaction happened on the surface of materials. After enlarge the concentration of Pt, higher amounts of electrons trapped by the finely dispersed Pt, the N—H bond dissociation is further promoted. Fig. 6(b) depicts the dot-line gas sensor response patterns toward different concentration of ammonia in the range of 50–1500 ppm. The trend is that the response of each sensor increases with the increasing tested gas concentration and the increasing Pt loaded concentration. These phenomena including the higher response and lower optimum operating temperature are thought to be the typical characteristics of noble metal activation in gas sensing performance, which in turn directly verifies the promotion effect of Pt functionalization [31,33]. In addition, the gas response of larger Pt concentration loaded on the mesoporous WO_3 towards NH_3 was depicted in Fig. S1†.

Fig. 7(a) displays dynamic resistance curve of pure mesostructured WO_3 towards different ammonia concentrations from 50 to 1500 ppm at 200 °C. In Fig. 7(a), the gas resistance has an abrupt decrease followed by a slow increase when ammonia is introduced. Then, when the sensor exposed to ambient air again, the resistance sharply increased. However, it has a higher value than

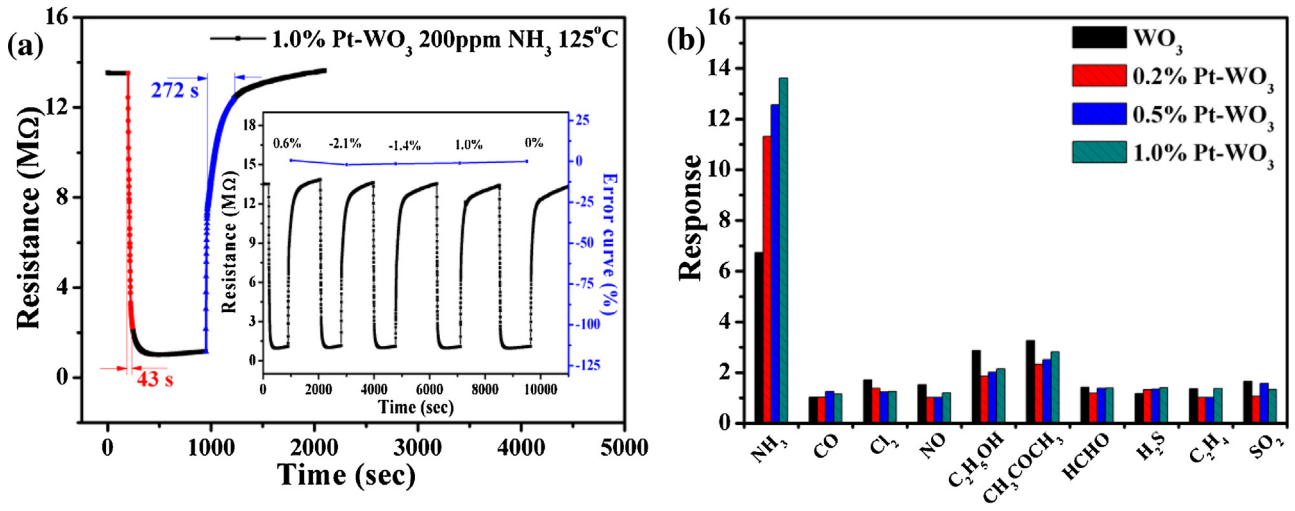

Fig. 9. (a) Response-recovery detail pattern of 1.0% Pt-loaded WO_3 towards 200 ppm ammonia at 125 °C with dynamic response-recovery cycles to 200 ppm ammonia inset, (b) the gas response of obtained samples toward different gases with a concentration of 200 ppm at 125 °C.

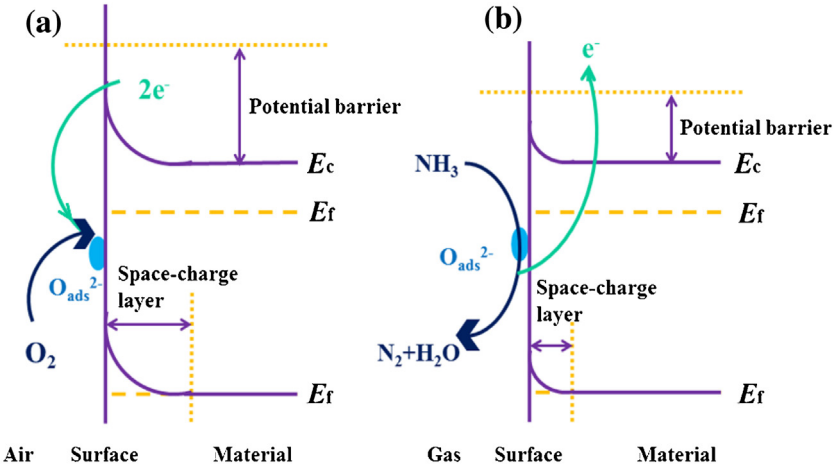

Fig. 10. Schematic drawing of the reaction mechanism towards obtained material based sensor in (a) air and (b) ammonia.

before NH_3 introduced again and then with a slow recovery to initial value. These phenomenon can be related to the formation of NO_x due to the oxidation of NH_3 in the sensing process. When ammonia is introduced, sensor resistance decreases as adsorbed oxygen species (O^-, O^{2-}) is consumed. Meanwhile, NO_x may be produced at high temperature [34] ($2NH_3 + 5O^- \rightarrow 2NO + 3H_2O + 5e^-$, $2NH_3 + 4O^- \rightarrow N_2O + 3H_2O + 4e^-$) which may trap electrons, form NO_x^- species, and lead to the increase of resistance. However, when ammonia is removed, oxygen is quickly adsorbed on the surface, which makes sensor resistance increase. The hard desorbed NO_x^- species [35] makes the recovery resistance higher than the original value. Fig. 7(b) demonstrates the dynamic response-recovery pattern of 1% Pt-loaded mesoporous WO_3 to different ammonia concentrations from 50 to 1500 ppm at 125 °C. As shown in Fig. 7(b), the gas response rapidly increases and decreases in response and recovery situations, respectively. The gas response increase with the increasing concentration of ammonia. At the relatively low temperature compared with 200 °C, unlike the case of pure mesoporous WO_3, finely dispersed Pt may acts as catalyst of the interaction between ammonia and O_o centers [36], decreasing the activation barrier and promoting the dissociation of the N—H bond. Under the lower temperature of 125 °C, there is not enough thermal activation to produce NO_x species who can trap electrons. As a result, the unsatisfactory dynamic sensor response phenomenon eliminated and good response-recovery properties can be observed.

The response and recovery time of the gas sensor are significant parameters in the fields of harmful and toxic gas detection. Fig. 8 depicts the variation in response and recovery time as a function of temperature for the obtained mesoporous samples toward 200 ppm of ammonia. The response and recovery time decreases with increase in temperature for all prepared materials. This is attributed to the fast adsorption and desorption of gas molecules on the sensor surface at higher temperature. After loading Pt on mesoporous WO_3, the response and recovery speed becomes faster, which indicates the catalysis of Pt. The response-recovery detail of 1.0% Pt-loaded WO_3 towards 200 ppm ammonia at 125 °C is revealed in Fig. 9(a). As depicted, the response and recovery time is 43 s and 272 s, respectively. The long recovery time may be attributed to the mesoporous structure which slow down the desorption rate of detected gas, and this phenomenon is also observed in mesoporous In_2O_3 [37].

The 1.0% Pt-loaded WO_3 was investigated by testing 200 ppm of ammonia for five times under the same condition to evaluate the repeatability properties, and the dynamic response-recovery cycles are present in the inset of Fig. 9(a). The gas resistance curve presents the similar continuous recycles and the error is limited in the range of 3%. These factors reveal the sensor based on Pt-loaded

Table 2
Comparison of the gas-sensing performance of various oxide based sensors toward ammonia.

Sample	T (°C)	C (ppm)	S (R_a/R_g)	Refs.
1.0% Pt-WO_3	125	200	13.61	This work
Hierarchical SnO_2	200	300	6	[38]
Mesoporous SnO_2	260	500	5	[39]
2.0% V-WO_3	700	500	14	[40]
WO_3 nanofiber	200	100	5.5	[41]

WO_3 has good repeatability. The selectivity of obtained samples to 200 ppm of different test gases is carried out in Fig. 9(b). It is obvious that the sensitivity to ammonia is higher than that of other gases for the fabricated gas sensors. Compared with pure mesoporous WO_3, Pt-loaded mesoporous WO_3 materials enhance the sensitivity towards NH_3 and present little change towards other gases. This means that the Pt-loaded WO_3 enhanced the selectivity to ammonia. Comparison of the gas sensing performance of various gas sensors to ammonia in other researches is displayed in Table 2.

The ammonia gas sensing mechanism of the fabricated sensor is based on the changed conductance, which can be depicts by Wolkentein's model [3] as shown in Fig. 10. It is generally accepted that the charged species such as O^-, O^{2-} are adsorbed on the surface of metal oxide in air through capturing free electrons from the sensing materials. Leading to the formation of a thick space charged layer and a consequently high resistance of the sensor. Once the sensor is in the exposure to ammonia, the ammonia will react with the adsorbed oxygen species and the released the captured electrons, resulting in a thin space charged layer and the decrease of the resistance.

Pt-loaded mesoporous WO_3 presents the enhanced gas sensing performance which is attributed to the catalyst and the matrix. The enhancement caused by Pt can be explained by catalytic promotion. When the mesoporous material is loaded with uniformly distributed Pt on over the surface, Pt acts as the efficient catalyst for adsorption-desorption reactions of oxygen and ammonia gas [36] and catalyzes the conversion of ammonia as a pretreatment. In case of catalytic reaction, the ammonia is first adsorbed on a catalyst (Pt), gets split up into ions, then spills over on the surface, and reacts with surface oxygen ions on the sensor material, thereby decreasing the resistance of the sensor and enhancing the response [42]. The matrix with mesoporous structure promotes the diffusion and transport ammonia into the sensing layer, and this effect, together with the electronic sensitization promoted by the Pt catalyst located on the surface, further enhances the gas sensitivity of the material.

4. Conclusion

Mesoporous WO_3 and Pt-loaded mesoporous WO_3 have been successfully prepared by nanocasting method. The obtained materials presented highly ordered mesostructure with a high specific surface area (85.8 $m^2\ g^{-1}$), which is convenience for gas diffusion and can provide more active sites. It was found that Pt-loaded materials enhance the sensitivity significantly toward ammonia. Apart from the outstanding response, the Pt-loaded WO_3 also present good response-recovery properties, repeatability and selectivity. Furthermore, Pt-loaded materials decrease the operating temperature, from 200 °C to 125 °C, and the sensitivity achieves to 13.6. The enhancement of the gas sensing properties is attributed to the effect of the matrix and the catalyst Pt. Pt acted as catalyst decreasing the resistance of the sensor and enhancing the response. It demonstrates that the Pt-loaded mesoprous WO_3 is an excellent ammonia gas sensing material of chemical sensors.

Acknowledgements

This work was supported by the National Nature Science Foundation of China (61304242 and 61327804), National High-Tech Research and Development Program of China (863 Program, Nos. 2013AA030902 and 2014AA06A505), China Postdoctoral Science Foundation (No.2013M530979), Science and Technology Development Program of Jilin Province (No. 20150520091JH).

Appendix A. Supplementary data

Supplementary data associated with this article can be found, in the online version, at http://dx.doi.org/10.1016/j.snb.2016.07.085.

References

[1] D.D. Nguyen, D.V. Dang, D.C. Nguyen, Hydrothermal synthesis and NH_3 gas sensing property of WO_3 nanorods at low temperature, Adv. Nat. Sci.: Nanosci. Nanotechnol. 6 (2015) 035006 (6pp).
[2] B. Timmer, W. Olthuis, A.V. berg, Ammonia sensors and their applications-a review, Sens. Actuators B 107 (2005) 666–677.
[3] X. Liu, N. Chen, B. Han, X. Xiao, G. Chen, I. Djerdj, Y. Wang, Nanoparticle cluster gas sensor: Pt activated SnO_2 nanopaticles for NH_3 detection with ultrahigh sensitivity, Nanoscale 7 (2015) 14872–14880.
[4] T. Zhang, M.B. Nix, B.Y. Yoo, M.A. Deshusses, N.V. Myung, Electrochemically functionalized single-walled carbon nanotube gas sensor, Electroanalysis 18 (2006) 1153–1158.
[5] Y.S. Lee, B.S. Joo, N.J. Choi, J.O. Lim, J.S. Huh, D.D. Lee, Visible optical sensing of ammonia based on polyaniline film, Sens. Actuators B: Chem. 93 (2003) 148–152.
[6] S. Christie, E. Scorsone, K. Persaud, F. Kvasnik, Remote detection of gaseous ammonia using the near infrared transmission properties of polyaniline, Sens. Actuators B: Chem. 90 (2003) 163–169.
[7] C.Y. Shen, S.Y. Liou, Surface acoustic wave gas monitor for ppm ammnia detection, Sens. Actuators B: Chem. 131 (2008) 673–679.
[8] V.B. Raj, A.T. Nimal, Y. Parmar, M.U. Sharma, K. Sreenivas, V. Gupta, Cross-sensitivity and selectivity studies on ZnO surface acoustic wave ammonia sensor, Sens. Actuators B: Chem. 147 (2010) 517–524.
[9] Y. Zhang, P. Xu, J. Xu, H. Li, W. Ma, NH_3 sensing mechanism investigation of CuBr: different complex interaction of Cu^+ ion with NH_3 and O_2 molecules, J. Phys. Chem. C 115 (2011) 2014–2019.
[10] P. Lauque, M. Bendahan, J.L. Seguin, K.A. Ngo, P. Knauth, Highly sensitive and selective room temperature NH_3 gas microsensor using an ionic conductor (CuBr) film, Anal. Chim. Acta 515 (2004) 279–284.
[11] Y.K. Chung, M.H. Kim, W.S. Um, H.S. Lee, J.K. Song, S.C. Choi, K.M. Yi, M.J. Lee, K.W. Chung, Gas sensing properties of WO_3 thick film for NO_2 gas dependent on process condition, Sens. Actuators B: Chem. 60 (1999) 49–56.
[12] Q. Qi, P.P. Wang, J. Zhao, L.L. Feng, L.J. Zhou, R.F. Xuan, Y.P. Liu, G.D. Li, SnO_2 nanoparticle-coated In_2O_3 nanofibers with improved NH_3 sensing properties, Sens. Actuators B: Chem. 194 (2014) 440–446.
[13] A. Ponzoni, E. Comini, M. Ferroni, G. Sberveglieri, Nanostructured WO_3 deposited by modified thermal evaporation for gas sensing applications, Thin Solid Films 490 (2005) 81–85.
[14] N. Pinna, M. Niederberger, Surfactant-free nonaqueous synthesis of metal oxide nanostructures, Angew. Chem. Int. Ed. 47 (2008) 5292–5304.
[15] Z.G. Zhao, M. Miyauchi, Shape modulation of tungstic acid and tungstic oxide hollow structures, J. Phys. Chem. C 113 (2009) 6539–6546.
[16] S. Zhu, X. Liu, Z. Chen, C. Liu, C. Feng, J. Gu, Q. Liu, D. Zhang, Synthesis of Cu-doped WO_3 materials with photonic structures for high performance sensors, J. Mater. Chem. 20 (2010) 9126–9132.
[17] J.H. Lee, Gas sensors using hierarchical and hollow oxide nanostructures: overview, Sens. Actuators B: Chem. 140 (2009) 319–336.
[18] H. Zheng, J.Z. Ou, M.S. Strano, R.B. Kaner, A. Mitchell, K. Kalantar-zadeh, Nanostructured tungsten oxide-properties, synthesisi, and applications, Adv. Funct. Mater. 21 (2011) 2175–2196.
[19] Q. Xiang, G.F. Meng, H.B. Zhao, Y. Zhang, H. Li, W.J. Ma, J.Q. Xu, Au nanoparticle modified WO_3 nanorods with their enhanced properties for photocatalysis and gas sensing, J. Phys. Chem. C 114 (2010) 2049–2055.
[20] A. Kolmakov, D.O. Klenov, Y. Lilach, S. Stemmer, M. Moskovits, Enhanced gas sensing by individual SnO_2 nanowires and nanobelts functionalized with Pd catalyst particles, Nano Lett. 5 (2005) 667–673.
[21] A. Boudiba, C. Zhang, C. Navio, C. Bittencourt, R. Snyders, M. Debliquy, Preparation of highly selective, sensitive and stable hydrogen sensors based on Pd-doped tungsten trioxide, Procedia Eng. 5 (2010) 180–183.
[22] M.D. Arienzo, M. Crippa, P. Gentile, C.M. Mari, S. Polizzi, R. Ruffo, R. Scotti, L. Wahba, F. Morazzoni, Sol-gel derived mesoporous Pt and Cr-doped WO_3 thin films: the role played by mesoporosity and metal doping in enhancing the gas sensing properties, J. Sol Gel Sci. Technol. 60 (2011) 378–387.
[23] M.D. Arienzo, L. Armelao, A. Cacciamani, C.M. Mari, S. Polizzi, R. Ruffo, R. Scotti, A. Testino, L. Wahba, F. Morazzoni, One-step preparation of SnO_2 and

Pt-doped SnO_2 as inverse opal thin films for gas sensing, Chem. Mater. 22 (2010) 4083–4089.
[24] Y. Wang, X. Cui, Q. Yang, J. Liu, Y. Gao, P. Sun, G. Lu, Preparation of Ag-loaded mesoporous WO_3 and its enhanced NO_2 sensing performance, Sens. Actuators B: Chem. 225 (2016) 544–552.
[25] T. Waitz, T. Wagner, T. Sauerwald, C.D. Kohl, M. Tiemann, Ordered mesoporous In_2O_3: synthesis by structure replication and application as a methane gas sensor, Adv. Funct. Mater. 19 (2009) 653–661.
[26] C. Karunakaran, P. Anilkumar, P. Gomathisankar, Photoproduction of iodine with nanoparticulate semiconductors and insulators, Chem. Cent. J. 5 (2011) 31.
[27] H.W. Kim, H.G. Na, D.S. Kwak, H.Y. Cho, Y.J. Kwon, Enhanced gas sensing characteristics of Ag_2O-functionalized net worked In_2O_3 nanowirea, Jpn. J. Appl. Phys. 52 (2013) 10MD01.
[28] B.H. Jang, O. Landau, S.J. Choi, J. Shin, A. Rothschild, I.D. Kim, Selectivity enhancement of SnO_2 nanofiber gas sensors by functionalization with Pt nanocatalysts and manipulation of the operation temperature, Sens. Actuators B: Chem. 188 (2013) 156–168.
[29] M.D. Arienzo, L. Armedao, C.M. Mari, S. Polizzi, R. Ruffo, R. Scotti, F. Morazzi, Macroporous WO_3 thin films active in NH_3 sensing: role of the hosted Cr isolated centers and Pt nanoclusters, J. Am. Chem. Soc. 133 (2011) 5296–5304.
[30] L. Gao, F. Ren, Z. Cheng, Y. Zhang, Q. Xiang, J. Xu, Porous corundum-type In_2O_3 nanoflowers: controllable synthesis, enhanced ethanol-sensing properties and response mechanism, Cryst. Eng. Comm. 17 (2015) 3268–3276.
[31] C. Dong, X. Liu, X. Xiao, G. Chen, Y. Wang, I. Djerdj, Combustion synthesis of porous Pt-functionalized SnO_2 sheets for isopropanol gas detection with a significant enhancement in response, J. Mater. Chem. A 2 (2014) 20089–20095.
[32] Y.V. Kaneti, Z. Zhang, J. Yue, Q.M.D. Zakaria, C. Chen, X. Jiang, et al., Crystal plane dependent gas-sensing properties of zinc oxide nanostructures: experimental and theoretical studies, Phys. Chem. Chem. Phys. 16 (2014) 11471–11480.
[33] M. Shahabuddin, A. Sharma, J. Kumar, M. Tomar, A.U. Umar, V. Gupta, Metal clusters activated SnO_2 thin film for low level detection of NH_3 gas, Sens. Actuators B: Chem. 194 (2014) 410–418.
[34] J.M. Gallardo, V. Sanchez, G. Ramis, G. Busca, An FT-IR study of ammonia adsorption and oxidation over anatase-supported metal oxides, Appl. Catal. B 13 (1997) 45–58.
[35] Y. Takao, K. Miyazaki, Y. Shimizu, M. Egashira, High ammonia sensitive semiconductor gas sensor with double-layer structure and interface electrodes, J. Electrochem. Soc. 141 (1994) 1028–1034.
[36] K. Mudiyanselage, M. Trenary, Kinetics of NH formation and dissociation on Pt (111), J. Phys. Chem.: C 111 (2007) 7127–7136.
[37] X. Sun, H. Hao, H. Ji, X. Li, S. Cai, C. Zheng, Nanocasting synthesis of In_2O_3 with appropriate mesostructured ordering and enhanced gas-sensing property, ACS Appl. Mater. Interfaces 6 (2014) 401–409.
[38] L.V. Thong, L.T.N. Loan, N.V. Hieu, Comparative study of gas sensor performance of SnO_2 nanowires and their hierarchical nanostructures, Sens. Actuators B: Chem. 150 (2010) 112–119.
[39] W. Guo, X. Duan, Y. Shen, K. Qi, C. Wei, W. Zheng, Ionothermal synthesis of mesoporous SnO_2 nanomaterials and their gas sensitivity depending on the reducing ability of toxic gases, Phys. Chem. Chem. Phys. 15 (2013) 11221–11225.
[40] I. Jiménez, A.M. Vilà, A.C. Calveras, J.R. Morante, Gas-sensing properties of catalytically modified WO_3 with copper and vanadium for NH_3 detection, IEEE Sens. J. 5 (2005) 385–391.
[41] J. Leng, X. Xu, N. Lv, H. Fan, T. Zhang, Synthesis and gas-sensing characteristics of WO_3 nanofibers via electrospinning, J. Colloid Interface Sci. 356 (2010) 54–57.
[42] V. Srivastava, K. Jain, Highly sensitive NH_3 sensor using Pt catalyzed silica coating over WO_3 thick films, Sens. Actuators B: Chem. 133 (2008) 46–52.

Biographies

Yinglin Wang received the MS degree in polymer chemistry and physics from Changchun University of Technology in 2014. She is currently studying for her Dr. Eng. degree in College of Electronic Science and Engineering, Jilin University. Her research interests include the synthesis of mesoporous materials and their applications in gas sensors.

Jie Liu received her BE degree from Jilin University of China in 2015. She is currently working toward the MS degree in the Electronics Science and Engineering department, Jilin University. Her current research is focus on the preparation and application of graphene and semiconductor oxide, especial in gas sensor.

Xiaobiao Cui received the BE degree in Department of Electronic Sciences and Technology in 2013. He is currently working toward the MS degree in the Electronics Science and Engineering department, Jilin University. His research interests include the synthesis of carbon dots and their applications.

Yuan Gao received her PhD degree from Department of Analytical Chemistry at Jilin University in 2012. Now she is an associate professor in Jilin University, China. Her current research is focus on the preparation and application of graphene and semiconductor oxide, especial in gas sensor and biosensor.

Jian Ma is engaged in the synthesis and characterization of the semiconducting functional materials and gas sensors.

Yanfeng Sun obtained his PhD from Jilin University of China in 2007. Presently, he is working as associate professor in Electronics Science and Engineering Department of Jilin University. His current research interests are nanoscience and gas sensors.

Peng Sun received his PHD degree from Jilin University of China in 2014. Now, he is engaged in the synthesis and characterization of the semiconducting functional materials and gas sensors.

Xishuang Liang received the B. Eng. degree in Department of Electronic Science and Technology in 2004. He received his Doctor's degree in College of Electronic Science and Engineering at Jilin University in 2009. Now he is an associate professor of Jilin University, China. His current research is solid electrolyte gas sensor.

Tong Zhang is a professor of Jilin University, China. Her current research interests include the development of chemical sensors and the application of the function materials.

Geyu Lu received the B. Sci. degree in electronic sciences in 1985 and the M. Sci. degree in 1988 from Jilin University in China and the Dr. Eng. degree in 1998 from Kyushu University in Japan. Now he is a professor of Jilin University, China. His current research interests include the development of chemical sensors and the application of the function materials.